Coagulation at the blood-electrode interface: the role of electrochemical desorption and degradation of fibrinogen

Simona, Benjamin R ; Brunisholz, René A ; Morhard, Robert ; Hunziker, Peter ; Vörös, János

Abstract: The influence of electrochemistry on the coagulation of blood on metal surfaces was demonstrated several decades ago. In particular, the application of cathodic currents resulted in reduced surface thrombogenicity, but no molecular mechanism has been so far proposed to explain this observation. In this article we used for the first time the quartz crystal microbalance with dissipation monitoring technique coupled with an electrochemical setup (EQCM-D) to study thrombosis at the blood-electrode interface. We confirmed the reduced thrombus deposition at the cathode, and we subsequently studied the effect of cathodic currents on adsorbed fibrinogen (Fg). Using EQCM and mass spectrometry, we found that upon applying currents Fg desorbed from the electrode and was electrochemically degraded. In particular, we show that the flexible N-terminus of the -chain, containing an important polymerization site, was cleaved from the protein, thus affecting its clottability. Our work proposes a molecular mechanism that at least partially explains how cathodic currents reduce thrombosis at the blood-electrode interface and is a relevant contribution to the rational development of medical devices with reduced thrombus formation on their surface.

DOI: https://doi.org/10.1021/la500634y

COAGULATION AT THE BLOOD-ELECTRODE INTERFACE: THE ROLE OF ELECTROCHEMICAL DESORPTION AND DEGRADATION OF FIBRINOGEN

By Simona BR[1], Brunisholz RA[2], Morhard R[1], Hunziker P[2], Vörös J[1*]

Published in Langmuir, 30(24):7227-34 (2014). DOI: 10.1021/la500634y

1. Laboratory of Biosensors and Bioelectronics, Institute for Biomedical Engineering, University and ETH Zurich, Gloriastrasse 35, CH-8092 Zurich, Switzerland.
2. Functional Genomics Center Zurich, University and ETH Zurich, Winterthurerstrasse 190, CH-8057 Zurich, Switzerland.

Corresponding Author:

*Tel +41 (0) 44 632 59 03; Fax +41 (0) 44 632 11 93; e-mail: janos.voros@biomed.ee.ethz.ch (J.V.).
Notes: The authors declare no competing financial interest.

ABSTRACT

The influence of electrochemistry on the coagulation of blood on metal surfaces was demonstrated several decades ago. In particular, the application of cathodic currents resulted in reduced surface thrombogenicity, but no molecular mechanism has been so far proposed to explain this observation. In this article we used for the first time the quartz crystal microbalance with dissipation monitoring technique coupled with an electrochemical setup (EQCM-D) to study thrombosis at the blood–electrode interface. We confirmed the reduced thrombus deposition at the cathode, and we subsequently studied the effect of cathodic currents on adsorbed fibrinogen (Fg). Using EQCM and mass spectrometry, we found that upon applying currents Fg desorbed from the electrode and was electrochemically degraded. In particular, we show that the flexible N-terminus of the α-chain, containing an important polymerization site, was cleaved from the protein, thus affecting its clottability. Our work proposes a molecular mechanism that at least partially explains how cathodic currents reduce thrombosis at the blood–electrode interface and is a relevant contribution to the rational development of medical devices with reduced thrombus formation on their surface.

INTRODUCTION

Over the past decades a considerable effort has been made to develop surfaces with minimally thrombogenic properties for endovascular devices such as stents, catheters, filters, sensors, and many others. The formation of a thrombus resulting from the contact of blood with the implant's surface represents a risk from a medical perspective (thromboembolism) and from an engineering perspective (implant failure).[1, 2] The major difficulty that scientists and engineers face in the development of "more hemocompatible" blood-contacting devices is the limited understanding of the phenomenon of contact activation of blood coagulation and the lack of a paradigm capable of explaining all empirical observations.[3] Consequently, there is little or no consensus concerning the parameters to optimize in designing better surfaces.

The leading opinion states that protein adsorption at the implant's surface is the first step of a long series of events, including platelet adhesion and activation, finally leading to thrombosis.[4-6] Regardless of what strategy is pursued to reduce blood coagulation on a surface, it is crucial to determine the effect of the surface treatment on the adsorbed plasma protein layer. The understanding of this phenomenon is necessary, though possibly not sufficient, to rationally design and develop blood-contacting devices.

Various strategies have been used to control surface coagulation including coating the surface with protein-resistant polymers,(7-9) active molecules such as anticoagulants[10, 11] or fibrinolysis promoters,[12-15] endothelial cells[16, 17] or polymers mimicking their membrane,[18, 19] and last but not least inorganic thin films conferring various surface properties as reviewed by Mani and colleagues[20]. A strategy not comprised in this list was proposed by P. N. Sawyer more than 40 years ago and consisted in cathodically polarizing the implant's surface. Sawyer's pioneering work demonstrated that thrombogenic metals had reduced clotting at their surface upon application of cathodic potentials *in vivo*.[21, 22] In contrast, anodic surfaces were associated with accelerated thrombus formation.[23] The authors suggested that the electrochemical reactions occurring at the electrode surface involving the plasma protein fibrinogen (Fg) could partially explain these observations. A large part of the studies on hemocompatibility focused on Fg because it constitutes the building block of the polymeric scaffold of a blood clot (fibrin), because of its high capacity to activate platelets, and because surfaces precoated with Fg, among other proteins, showed increased surface-induced thrombogenesis.[24-26]

At anodic potentials Fg is electropolymerized to form fibrin-like fibers, and this reaction might cause an acceleration of the coagulation process.[21, 27] At the cathode Fg was recently shown by fluorescence and atomic force microscopy to desorb from the electrode surface.[28] Sawyer recognized that an in-depth investigation of the nature of the Fg reduction products was necessary in order to understand what is the mechanism behind the reduced thrombus formation at cathodic potentials.[21]

In this article, we used for the first time the quartz crystal microbalance with dissipation monitoring technique coupled with an electrochemical setup (EQCM-D) to semiquantitatively study thrombosis at the cathode–blood plasma interface. We confirmed Sawyer's observation and found that Fg desorbs upon the application of cathodic currents in a current density-dependent manner. We also demonstrated using EQCM and mass spectrometry (MS) that the alkaline environment in proximity of the cathode causes the degradation of Fg. In particular, we found a low molecular weight (MW) Fg degradation product containing an important polymerization site (EA located at the α-chain N-terminus). The degradation of the α-chain N-terminus explains the impaired clottability of the cathodically desorbed Fg and the reduced thrombosis at the cathode's surface.

EXPERIMENTAL SECTION

Materials

Frozen anticoagulated human citrated blood plasma (CBP; ACD stabilized) was purchased from Blutspende Zürich (Zurich, Switzerland), and 1 mL aliquots were stored at −80 °C until use. Human fibrinogen (Fg; plasminogen, von Willebrand factor and fibronectin depleted, code FIB3) was purchased from Enzyme Research Laboratories Ltd. (Swansea, UK). Fg was dissolved during 4 h at 37 °C at a concentration of 50 mg/mL in phosphate-buffered saline 1X (PBS; pH 7.4, no $CaCl_2$ and no $MgCl_2$, Life Technologies Ltd., Paisley, UK, code 10010-015), and 50 µL aliquots were stored at −80 °C until use. Thrombin (>2000 u/mg, code T6884), sodium chloride (NaCl; 99.8%, code 71380), ethanol (C_2H_6O; 99.8%, code 02854), 2-propanol (C_3H_8O; 99.8%, code 34965), calcium chloride ($CaCl_2$; anhydrous, 96.0%, code C5670), trifluoroacetic acid (TFA, CF_3COOH; 99%, code T62200), and glutaraldehyde ($CH_2(CH_2CHO)_2$; 8% in H_2O, code G7526) were purchased from Sigma-Aldrich (St. Louis, MO). Acetonitrile (ACN, CH_3CN; hypergrade, code 100029) was purchased from Merck Millipore (Billerica, MA).

MALDI-MS matrix α-cyano-4-hydroxycinnamic acid (HCCA, $C_{10}H_7NO_3$; code 8201344) and MALDI-MS targets (MTP 384 TF AnchorChip target plate 800 µm) were purchased from Bruker Daltonics GmbH (Bremen, Germany). Deconex 12PA-x cleaner was purchased from Borer Chemie AG (Zuchwil, Switzerland). Cleaner "Cobas Integra" was purchased from Roche Diagnostics GmbH (Mannheim, Germany). Electrochemical experiments were performed using an Autolab PGSTAT 302N potentiostat–galvanostat and potential–current signals were monitored with a computer interface NOVA v1.9 (Metrohm Autolab, Utrecht, The Netherlands). Quartz crystal microbalance with dissipation monitoring (QCM-D) experiments were performed on a Q-Sense E4 (data acquired using Q-Soft software v2.5.15) using gold-coated sensors (100 nm gold layer thickness, 14 mm diameter, code QSX301) (Q-Sense, Västra Frölunda, Sweden). A custom-made transparent electrochemical QCM (EQCM) module (capacity 200 µL) was developed in house to directly inject the sample on the sensing surface and to clearly monitor eventual formation of gas bubbles during electrochemical experiments. The working electrode (WE) consisted of the gold-coated sensor and the counter/reference electrode (CE/RE) of a platinum wire (Alfa Aesar, Ward Hill, MA). The cell incorporated a cellulose acetate membrane (500 MWCO, Harvard Apparatus, Holliston, MA) separating the CE/RE and the WE (Supporting Information Figure S1).

Methods

Cleaning Procedures

Gold-coated sensors were reutilized and cleaned before every experiment as follows: the surface was gently wiped with a 100% polypropylene tissue soaked in Cobas cleaner (10 v/v % in Milli-Q water) and rinsed with Cobas cleaner. Subsequently, the surfaces were thoroughly rinsed with 2-propanol and Milli-Q water and dried using a nitrogen stream. Immediately before starting the experiment, the surface was oxygen plasma cleaned (1 min, 30 W) (PDC-32G, Harrick Plasma, Ithaca, NY). The EQCM-D modules were cleaned before and after the experiment with Deconex cleaner (4% v/v in Milli-Q water), rinsed with Milli-Q water, and finally dried using a nitrogen stream.

EQCM-D: Blood Plasma Coagulation on a Gold Cathode

After 15 min thawing at 37 °C, 200 µL of CBP was injected in the EQCM-D module maintained at 37 °C, and a baseline was acquired for approximately 10–15 min. Subsequently, the gold-coated sensor was cathodically polarized by applying a square pulse current in galvanostatic mode ($I = -1$ mA/cm^2, where I is the pulse amplitude; $\tau_{ON} = 1$ s where τ_{ON} is the pulse width and $\tau_{OFF} = 5$ s where τ_{OFF} is the inactive time). The control sample was left at open circuit potential (OCP). CBP was recalcified in order to trigger the coagulation process by injecting 20 µL of $CaCl_2$ (100 mM). The coagulation process was monitored via changes in frequency and dissipation.

Scanning Electron Microscopy (SEM)

Following the monitoring of CBP coagulation on a cathodically polarized gold surface using EQCM-D, the gold-coated sensors were removed from the EQCM-D modules and rinsed 3 times in PBS. Subsequently, the sensors were fixed in a 3% v/v solution of glutaraldehyde in PBS for 30 min at room temperature. Sample dehydration in a graded series of ethanol (from 30% to 95% v/v) and drying over the critical point of CO2 using a critical point dryer followed (CPD 030, Bal-Tec AG, Balzers, Liechtenstein). Dried samples were subsequently sputter-coated with a 5–10 nm layer of platinum (SCD500, Bal-Tec AG, Balzers, Liechtenstein). Finally, surfaces were imaged with a Supra 50 VP scanning electron microscope (Zeiss AG, Oberkochen, Germany) at 10 kV using secondary electron signals with a magnification between 1 and 10 000.

EQCM-D: Fg Electrochemical Desorption Studies

Fg was thawed 15 min at 37 °C and diluted in NaCl (100 mM) to a final concentration of 1 mg/mL. After acquisition of a baseline in NaCl (100 mM) for 10–15 min, 200 µL of Fg (1 mg/mL) was injected in the EQCM module maintained at 37 °C, and the adsorption of Fg on the gold surface was monitored. Once saturation of adsorbed Fg was reached, the chamber was rinsed 3 times by injecting 200 µL of NaCl (100 mM). Subsequently, the gold-coated sensor was cathodically polarized in galvanostatic mode by applying a constant current of $I = [-1000, -100, -80, -50, -10]$ µA/cm^2 or a square pulse current of $I = -1$ mA/cm^2 and $\tau_{ON} = [0.5, 1, 5]$ s and $\tau_{OFF} = 5$ s. The frequency and dissipation signals were monitored for approximately 15 min.

EQCM-D: Fg Degradation Studies and Fg Clottability

Fg was adsorbed on the gold surface as described in the previous paragraph. No rinsing steps were performed after the adsorption to have high Fg concentration (1 mg/mL) in the bulk. The gold surface was cathodically polarized ($I = -1$ mA/cm^2, dc) for 10 min. The control sample was left at OCP. Subsequently, the samples were collected from the EQCM module. In a first experiment, the collected samples were reinjected on clean gold crystals at OCP after baseline acquisition in NaCl (100 mM). To test for the Fg clottability, 20 µL of $CaCl_2$ (100

mM) was injected after baseline acquisition and 20 µL of thrombin (120 u/mL in PBS) was injected after saturation of Fg adsorption. In a second experiment, the collected samples were subjected to centrifugal filtration through a 30 kDa MWCO membrane following provider's instructions (Amicon Ultra-0.5 mL for protein purification, Merck Millipore, Billerica, MA). The filtrates were subsequently reinjected on clean gold crystals at OCP after baseline acquisition in NaCl (100 mM).

MALDI-TOF MS and MALDI-TOFTOF MS

The filtrates obtained by centrifugal filtration through a 30 kDa MWCO membrane (see previous paragraph) were concentrated by vacuum centrifugation (Savant SpeedVac SC110 equipped with RH40-11 rotor, Thermo Fisher Scientific Inc., Waltham, MA) for approximately 40 min. Subsequently, the concentrated samples were further concentrated and desalted using ZipTipC18 pipet tips (Merck Millipore, Billerica, MA) and eluted in 2 µL of a 1:1 solution of H_2O:ACN with 0.1% TFA. 1 µL of the eluted samples was spotted on the MALDI target followed by on-plate mixing with 1 µL of a 0.7 mg/mL HCCA matrix solution in 1:1 of H_2O:ACN with 0.1% TFA. Measurements were performed on the UltrafleXtreme spectrometer (Bruker Daltonics, Bremen, Germany). Protein fingerprints in the 500–5000 Da mass range were acquired, and peptides were analyzed via reflectron type measurement.

Data Analysis

QCM-D data were analyzed with Matlab 7.12.0 (The Math Works Inc., Natick, MA). The normalized frequency response was obtained by dividing the desorption curve by the adsorption saturation value. Only the third overtones are shown for sake of clarity. EQCM curves were acquired at least 3 times (single measurements and averages are shown). MS data were acquired using the FlexControl3.3 software, and the MS-MS spectra were matched to peptide sequences generated via in silico digestion (no enzyme, threshold 0.8–1.2) using the Sequence Editor of BioTools3.2 (Bruker Dalctonics, Bremen, Germany). The MS spectra were measured on four independent replicate samples without showing variations in the dominant peaks.

RESULTS AND DISCUSSION

EQCM and SEM: Blood plasma coagulation was reduced at the cathode surface

The QCM-D technique has been used in the past to study blood coagulation at the surface of various materials.[29-31] Here we used the QCM-D technique coupled with an electrochemical setup (EQCM-D) to semiquantitatively study the coagulation of human CBP on a cathodically polarized gold surface (Figure 1). After acquisition of a baseline in CBP, we recorded frequency and dissipation changes upon CBP recalcification. On the gold surface at OCP, we observed a 240 Hz frequency drop occurring approximately 15 min after the injection of $CaCl_2$ (Figure 1a). Simultaneously, we observed a 120×10^{-6} increase in dissipation Figure 1b). As previously described, these shifts are indicative of the formation of a blood clot on the sensor surface.[29, 30]

The application of a pulsed cathodic current ($I = -1$ mA/cm^2, $\tau_{ON} = 1$ s, $\tau_{OFF} = 5$ s) prior recalcification immediately caused a progressive increase of the frequency signal (Figure 1a), suggesting the desorption of plasma proteins from the surface, as later confirmed in Figure 2. We can exclude that this shift was due to permanent modifications of the gold substrate (e.g., delamination) because the same electric pulses applied in 100 mM NaCl did not cause a comparable frequency change (Supporting Information Figure S2). Approximately 15 min after the injection of $CaCl_2$ the frequency increase reversed probably because of the adsorption of fibrin fibers, resulting in a final 25 Hz net frequency drop (Figure 1a). The corresponding increase in dissipation was in the order of 50×10^{-6} (Figure 1b). The observed frequency and dissipation changes were approximately 10% and 40% of the signal shifts observed for the control surface, respectively.

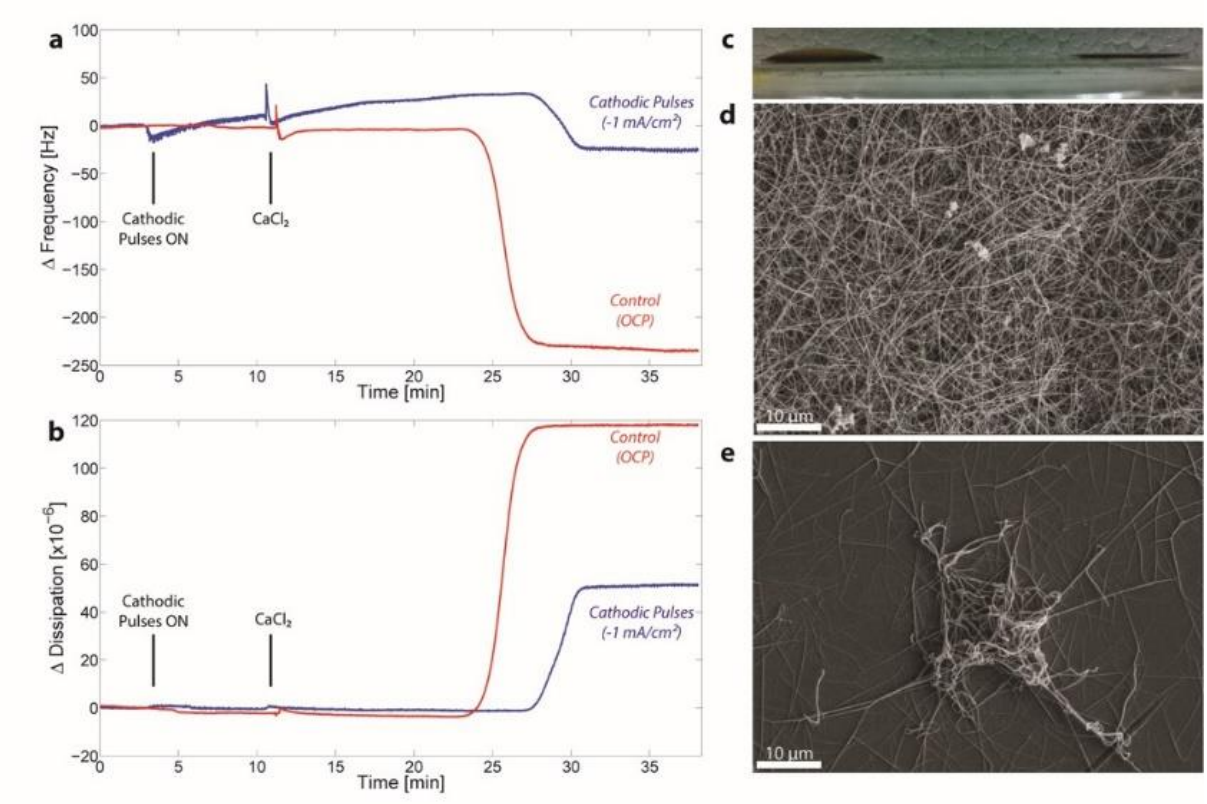

Figure 1. Citrated blood plasma (CBP) coagulation at the cathode's surface studied with EQCM-D and SEM. After baseline acquisition in CBP we applied cathodic pulses and subsequently injected $CaCl_2$ to trigger coagulation. The frequency (a) and the dissipation (b) signals showed reduced plasma coagulation upon the application of a pulsed cathodic current. (c) A photograph of the gold-coated sensors was taken (side view) after the experiment and showed a thick blood clot deposited onto the control surface at OCP (left side) while the polarized surface was clot-free (right side). The sensors were finally imaged at the SEM showing a densely packed fibrin network deposited onto the control surface (d) and a few isolated fibrin strands deposited onto the cathodically polarized surface (e).

Figure 1c shows the gold-coated crystals after the CBP recalcification experiment. The cathodically polarized surface appeared clean while the control surface was covered by a thick blood clot. SEM inspection revealed a homogeneous coverage of the control surface by a dense fibrin network (Figure 1d) and only isolated clusters of fibrin strands on the cathodically polarized gold surface (Figure 1e).

In summary, we showed that the coagulation of human CBP on a cathodically polarized gold surface was reduced compared to the coagulation on a non-polarized control surface. This result supported previous work done by P. N. Sawyer and colleagues, who demonstrated the influence of the interfacial potential of metal prostheses on their thrombogenicity and showed that metal surfaces maintained at cathodic potentials are characterized by an increased thromboresistance *in vivo*.[23] Efforts to understand the mechanisms responsible for this effect led researchers in the past to focus on the interfacial electrochemical reactions involving plasma proteins, in particular Fg.[21] The frequency increase observed immediately after the cathodic current onset in the CBP recalcification experiment (Figure 1a) led us to hypothesize that protein desorption from the cathode surface might partially explain the reduced deposition of fibrin fibers.

EQCM: Fg electrochemical desorption from a gold cathode as a function of current density

Figure 2a shows the 120 Hz frequency drop caused by the adsorption of Fg (1 mg/mL in 100 mM NaCl) on the gold surface and the subsequent signal recovery once we applied the cathodic dc ($I = -1$ mA/cm^2, for potential values refer to the Supporting Information Table S1). The recovery of the frequency signal to values close to the baseline in NaCl indicated the almost complete desorption of Fg upon the application of the cathodic current. Figure 2b shows the desorption curves obtained at different dc current densities. Figure 2c shows the desorption curves obtained using a square wave pulse current of −1 mA/cm^2 in I for different duty cycles. Our results showed that the desorption rate increased with increasing current density and increasing duty cycle. We observed an initial drop in frequency following the onset of the cathodic current (most likely due to current-induced protein

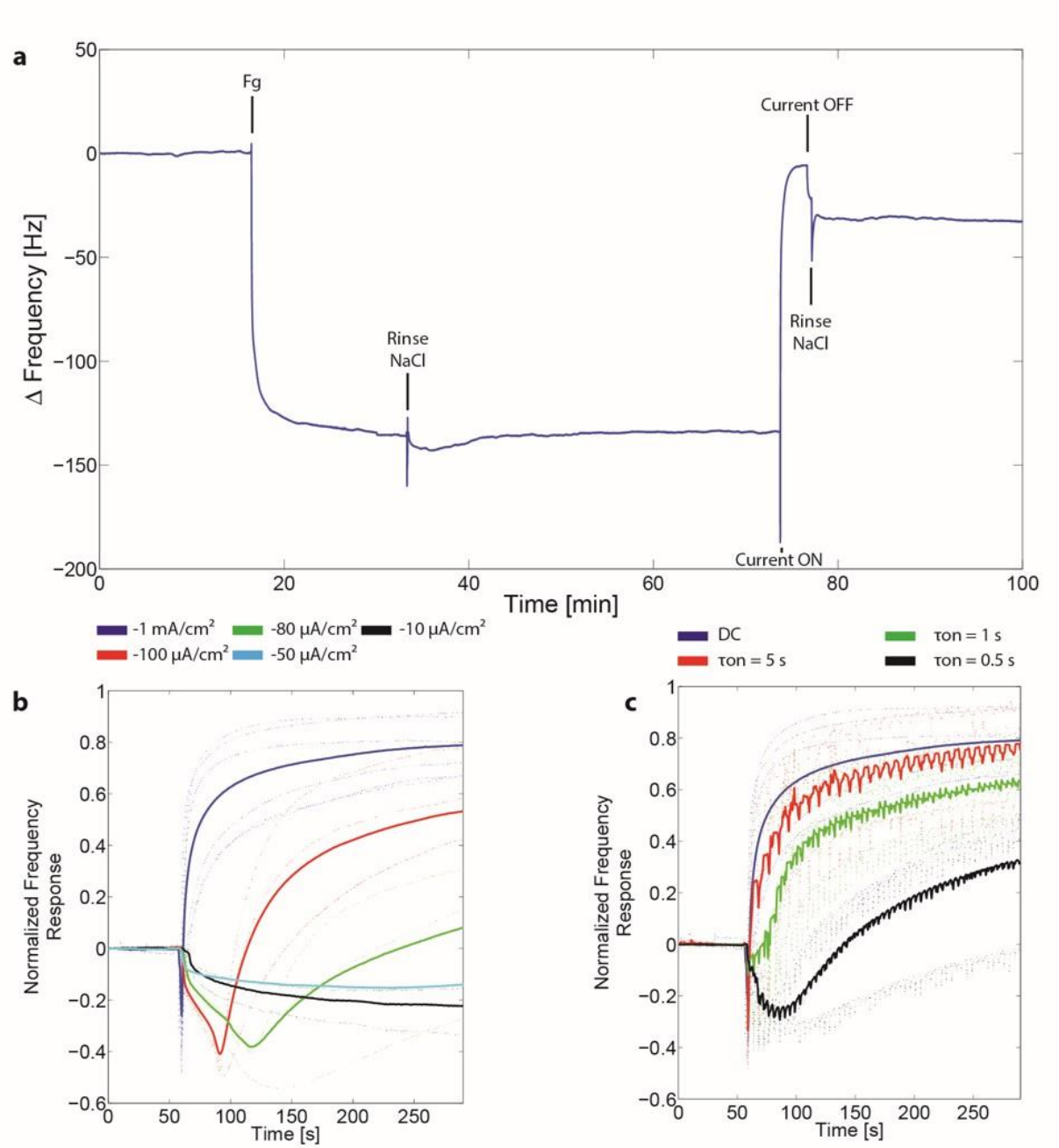

Figure 2. Dependency of Fg electrochemical desorption on current density. (a) After baseline acquisition in NaCl, Fg was adsorbed onto the gold surface, and once saturation was reached the chamber was rinsed with NaCl. Subsequently, a cathodic current was applied (−1 mA/cm^2, dc) and once the frequency signal recovered and stabilized close to baseline levels the current was switched off and the chamber rinsed with NaCl. (b) Fg desorption curves obtained with constant cathodic currents of various I. (c) Fg desorption curves obtained with pulsed cathodic current of I = −1 mA/cm^2 and various duty cycles. In (b, c) the bold curves are the averages of the single trials (dashed curves).

conformational changes on the surface) and a subsequent frequency increase if we applied a minimum current density of −80 µA/cm^2 (dc). Within 300 s, 80% of the Fg desorbed when the highest current density (i.e., −1 mA/cm^2 dc) was applied but only less than 20% removal was observed at −80 µA/cm^2. Interestingly, the average current density calculated for the lowest tested duty cycle (τ_{ON} = 0.5 s, τ_{OFF} = 5 s) is approximately −90 µA/cm^2, and the respective desorption curve is bounded by the curves obtained at dc current densities −80 and −100 µA/cm^2 (Supporting Information Figure S3), suggesting that the average current density is the parameter determining the desorption rate of Fg.

Our EQCM experiments supported the previous work of Mallon and co-workers showing Fg electrochemical desorption from a gold cathode using fluorescence and atomic force microscopy.[28] Additionally, our experiments showed the kinetics of the electrochemical desorption of Fg for different dc current densities and

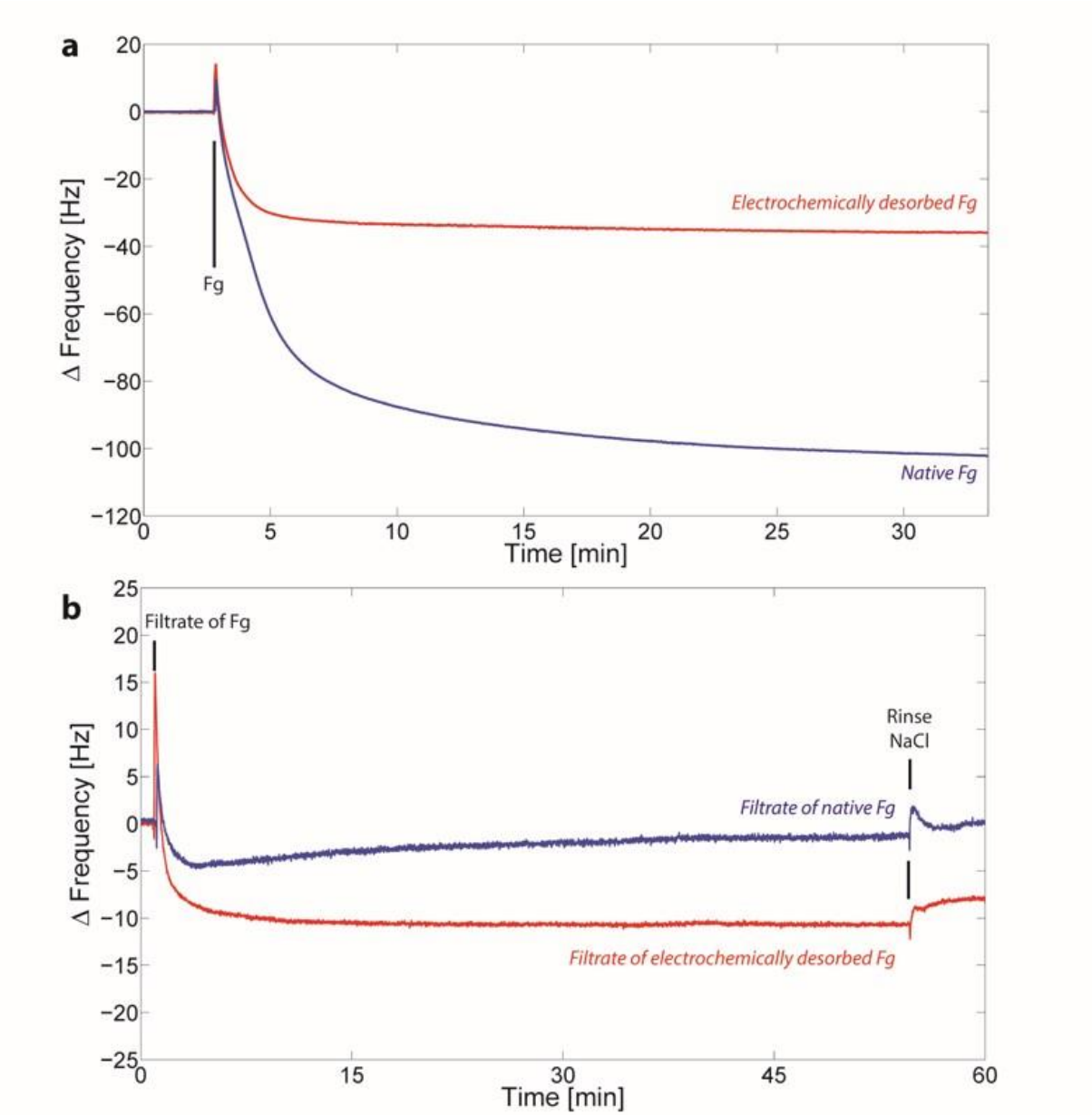

Figure 3. Readsorption of electrochemically desorbed Fg. (a) Previously desorbed Fg was readsorbed on a clean gold surface at OCP. The smaller frequency drop compared to the control Fg suggested that the MW of species in the solution decreased. (b) The previously desorbed Fg was filtered through a 30 kDa MWCO membrane and the filtrate subsequently readsorbed on a clean gold surface at OCP. The null frequency shift observed for the Fg control suggested that no species with MW smaller than the membrane cutoff were present in the solution. In contrast, the frequency drop observed for the electrochemically desorbed Fg suggested the presence of sub-30 kDa species in solution.

for a varying square pulse design. Fg desorption might explain previous ellipsometry and capacitance measurements revealing the decrease in Fg coverage with increased cathodic potentials.[21, 28]

EQCM: Readsorption of electrochemically desorbed Fg revealed Fg degradation

The elucidation of the nature of the electrochemically desorbed Fg might provide us with important insights about the reduced clot deposition at the cathode.[21] We therefore injected Fg in the EQCM chamber, monitored the adsorption, and without rinsing applied a cathodic dc ($I = -1$ mA/cm^2). The same process was performed for the control, only no current was applied. We performed desorption experiments in the presence of high Fg bulk concentration in order to obtain large amounts of electrochemically treated Fg for the subsequent analysis. The apparent desorption rate of Fg measured with the EQCM decreased if Fg remained in the bulk probably because both adsorption and desorption take place (not shown).

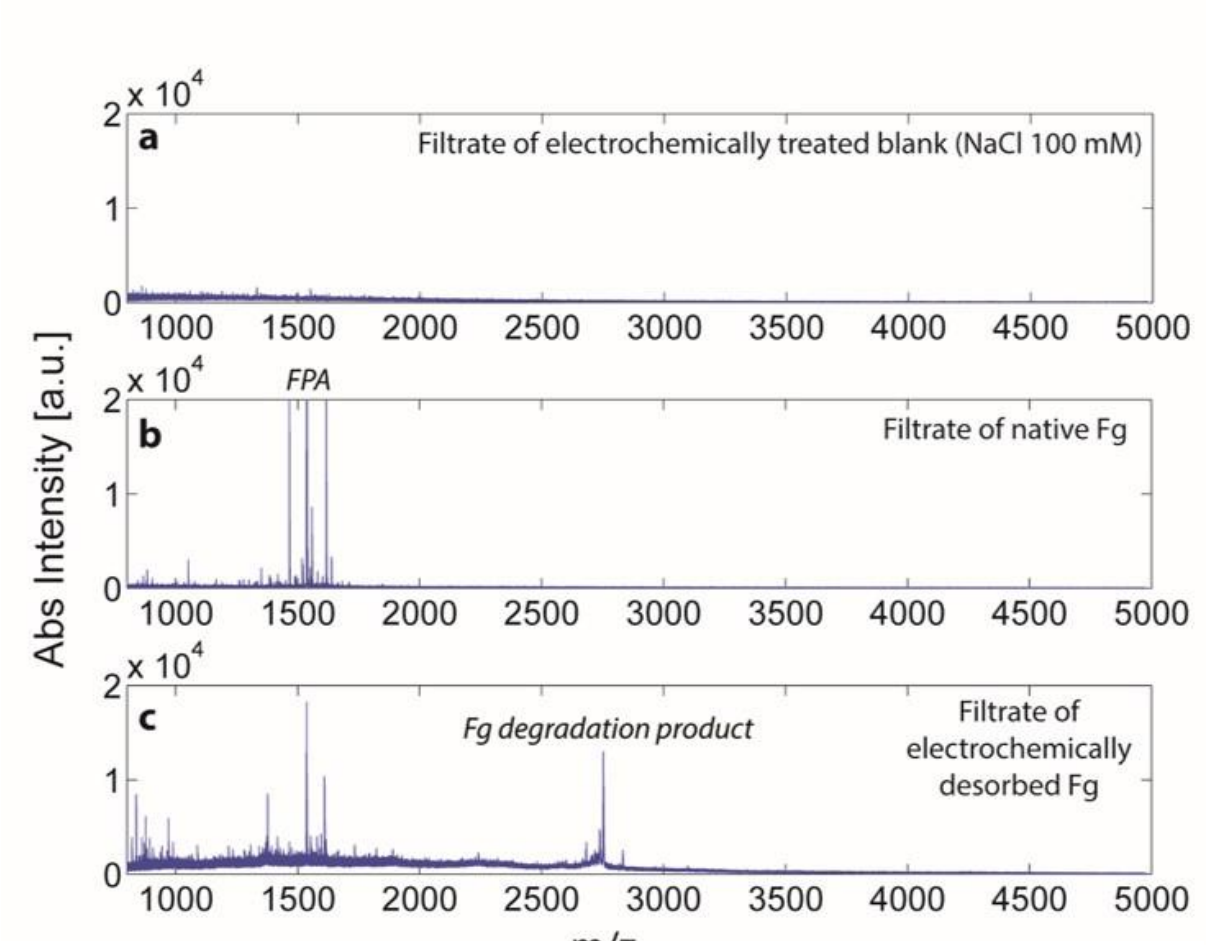

Figure 4. MALDI-TOF mass spectra of electrochemically desorbed Fg following filtration. (a) NaCl (blank) that was treated electrochemically in the same way as Fg to include any potential contamination and or leaching from the setup's components. (b) Spectrum of the controlled Fg filtrate showed three dominant peaks corresponding to the FPA (1536.7 Da) and its phosphorylated (1616.7 Da) and ragged versions (1465.7 Da). (c) Spectrum of the electrochemically desorbed Fg showed other peaks that were not present in the controls. In particular, we focused on the 2752.3 Da peak, which we referred to as electrochemically generated Fg degradation product.

After 10 min of electrochemical desorption we retrieved the content of the chamber and injected it into another QCM chamber containing a clean gold-coated crystal at OCP. Figure 3a shows the adsorption curves of the electrochemically desorbed Fg and the Fg that did not undergo electrochemical desorption. The readsorption of the electrochemically desorbed Fg resulted in a 30 Hz frequency shift whereas the readsorption of the Fg control resulted in a 100 Hz frequency shift comparable to the shift normally obtained for the first adsorption. Because the concentration of the two samples initially injected was the same and the chambers were not rinsed during the electrochemical experiment, the decreased frequency drop was due to the reduced MW of the species present in the electrochemically treated sample. We ensured that the cellulose acetate membrane separating the electrodes was not Fg permeable after the exposure to the electric currents, thus excluding Fg dilution.

Figure 3b shows the adsorption curves of the electrochemically desorbed and the native Fg after centrifugal filtration through a 30 kDa filter. As expected, the injection of the filtrate of the Fg control resulted in no frequency shift because the three Fg chains all have MWs larger than 30 kDa. In contrast, we observed a 10 Hz frequency shift for the electrochemically desorbed Fg, indicating the presence of species with a MW lower than the membrane cutoff but large enough to be observed with the QCM.

In summary, these results indicated that the electrochemically desorbed Fg was degraded, and standard proteomics techniques were subsequently used to further investigate the nature of the desorbed products.

MALDI-TOF MS: Mass determination of the sub-30 kDa Fg degradation products

Figure 4 shows the mass spectra of the sub-30 kDa filtrates obtained from the electrochemical desorption of Fg described above. The NaCl blank sample did not show any peak in the 800–5000 Da range (Figure 4a). This control was relevant to exclude the presence of contaminants in the solvents and possibly coming from the

leaching of the setup components during the electrochemical experiment. The native Fg control showed three dominant peaks at 1465.7, 1536.7, and 1616.7 Da (Figure 4b). The Fibrinopeptide A (FPA) has a mass of 1536.7 Da, and the peaks at 1465.7 and 1616.7 Da correspond to the FPA without the N-terminal Ala-20 and the phosphorylated FPA (phosphoserine present at position 22), respectively (the amino acid numeration in the text comprises the signaling peptide not present in the mature protein). Each Fg α-chain contains an N-terminal FPA which is cleaved by the enzyme thrombin to expose a polymerization site (E_A). This process starts the fibrillization process.[24] Interestingly, in the QCM experiment we did not observe the presence of the FPA (Figure 3b), possibly because of its too low concentration (MALDI samples were subjected to several preconcentration steps) or because of its too low MW. In addition to the FPA peaks, the electrochemically desorbed Fg presented a dominant peak at 2752.3 Da (Figure 4c). Because this peak was not present in the control samples, we concluded that this was a Fg degradation product of the electrochemical desorption. We further investigated the nature of these species using MALDI-TOFTOF MS.

MALDI-TOFTOF MS: The Fg degradation product contained the α-Chain N-Terminus polymerization site E_A

Using MALDI-TOFTOF MS, we determined that the peak at 2752.3 Da observed in the electrochemically desorbed Fg sample (Figure 4c) consisted of a 27 amino acid fragment of the mobile Fg α-chain N-terminus comprising the FPA (starting with Ala-20) and extending to the Ala-46 (Supporting Information Table S2 and Figure S4). This result suggested that a cleavage between the Ala-46 and the Cys-47 occurred upon the electrochemical desorption of Fg. Additionally, in this 2.7 kDa fragment we found the α-chain polymerization site EA Gly-Pro-Arg-Val (36–39). Finally, we confirmed that the peak at 1536.7 Da is the FPA (Supporting Information Table S3 and Figure S5).

Fg electrochemical degradation was previously reported using SDS-PAGE.[28] However, the low purity of the previously used Fg did not allow the identification of the low-MW degradation products observed in our study. Furthermore, the lack of an anodic and cathodic compartment separation (acetate cellulose membrane in our study) resulted in the inability to separately elucidate the nature of the anodically electropolymerized Fg and the cathodically degraded Fg.[21] This limitation is important for two reasons. First, a liquid chromatography–MS study showed that protein fragmentation can result from anodic oxidation.[32] Second, the anodic polymerization and the cathodic degradation of Fg have opposite effects on interfacial thrombosis, the first accelerating it[21, 33] and the second reducing it.

QCM-D: Electrochemical degradation of Fg resulted in impaired clottability

We addressed the functionality of the electrochemically degraded Fg. Figure 5 shows the clottability of the electrochemically desorbed Fg versus the clottability of the native Fg measured using the QCM-D. After the injection of the electrochemically desorbed Fg in the chamber, thrombin was added to trigger the polymerization. The polymerization of Fg resulted in a 200 Hz frequency drop and a simultaneous 18×10^{-6} dissipation increase. In contrast, the frequency and dissipation signals did not shift in response to the injection of thrombin into the electrochemically desorbed Fg solution, suggesting that the electrochemically desorbed Fg lost its clottability.

Our QCM-D and MS results allowed us to attribute the impaired clottability of Fg and the reduced clot deposition at the cathode surface at least partially to the electrochemical cleavage of the N-terminal flexible sequence of the α-chain (2.7 kDa) containing the polymerization site EA (as schematically represented in Figure 6).

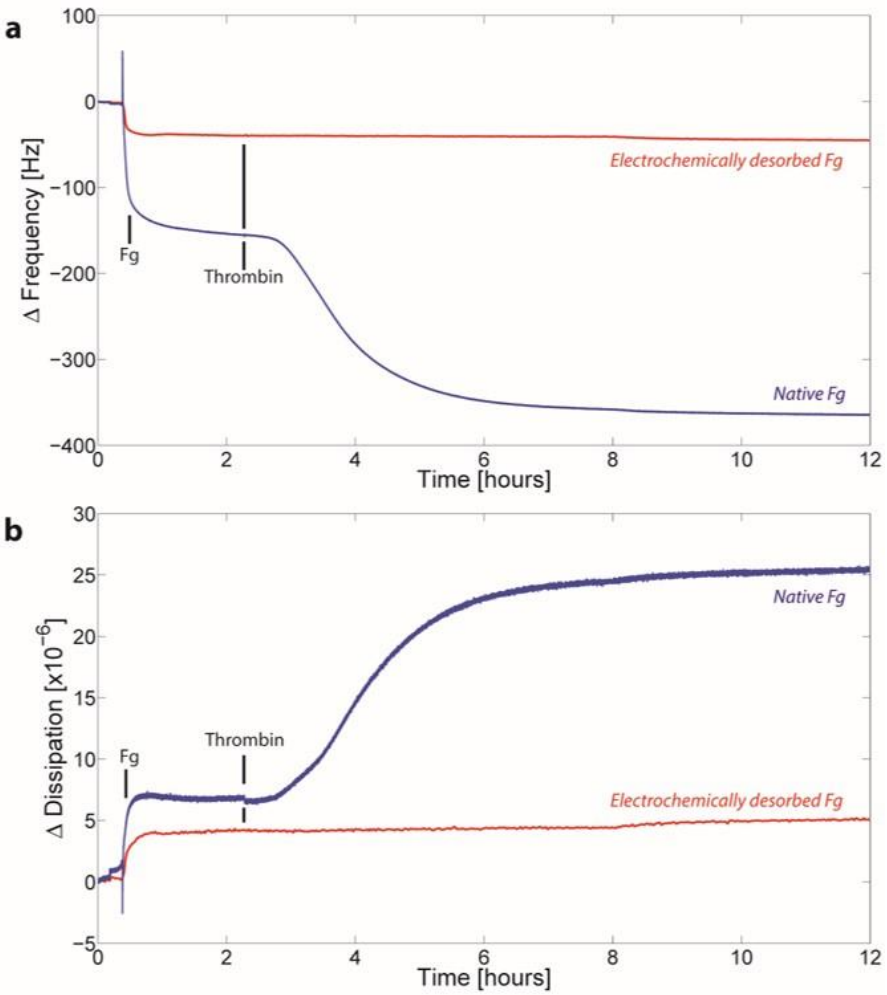

Figure 5. Clottability of electrochemically desorbed Fg. Electrochemically desorbed Fg was readsorbed onto a clean gold surface (OCP) after baseline acquisition in NaCl and $CaCl_2$. Once saturation was reached thrombin was injected to trigger the polymerization of Fg. The frequency signal (a) and the dissipation (b) signals did not change upon injection of thrombin for the electrochemically desorbed Fg. In contrast, the frequency and dissipation shifts observed for the native Fg control indicated Fg polymerization.

Possible mechanisms leading to the electrochemical desorption and degradation of Fg

Our final experiments were aimed at clarifying the mechanism(s) responsible for the electrochemical desorption of Fg from the cathode surface and for its degradation. Here we discuss three mechanisms that are likely to be involved in our observations. First, P. N. Sawyer and co-workers showed in previous potentiostatic and potentiodynamic studies of the interface between a Fg solution and a platinum electrode that the presence of Fg catalyzed the hydrogen evolution reaction at cathodic potentials (as reproduced in Supporting Information Figure S6). This was attributed to the electrolytic hydrogenation of Fg,[21, 34] which can lead to structural changes in the protein. We have limited information concerning site-specific electrocatalytic hydrogenation of proteins and peptides. The catalytic hydrogenation of aromatic amino acids is described in the literature. In particular, the indolyl group is sensitive to hydrogenolysis and this makes Tryptophan vulnerable to alteration due to hydrogenation.[35] However, our present work does not allow us to state if and which aromatic amino acids are involved in the observed Fg structural changes. Second, the alkaline environment forming in the proximity of the cathode due to electrolysis of water can result in alkali peptide hydrolysis. Previous work of our group addressed theoretically and experimentally the extent of pH changes resulting from electrolysis of water in the proximity of an indium tin oxide electrode.[36] To investigate the effect of an extreme alkaline environment on the Fg structure, here we prepared Fg solutions in 100 mM NaCl and added 200 mM NaOH. After overnight incubation at room temperature we neutralized the solution and performed centrifugal filtration through a 30 kDa MWCO membrane to analyze the filtrate using the QCM as previously done in Figure 3b. The

adsorption of the alkali treated Fg filtrate resulted in a 10 Hz frequency shift and supported the hypothesis of alkali peptide hydrolysis as a possible mechanism explaining the electrochemical desorption and degradation of Fg (Supporting Information Figure S7). The easy accessibility of the flexible α-chain N-terminus region to the aggressive environment might make it especially susceptible to cleavage. However other Fg regions not identified in our work might be degraded. It is important to mention that interfacial pH changes affect the structure and function of other blood coagulation factors not studied in this work. As most of enzymes, thrombin and factor XIII show pH-dependent activity,[37, 38] and we recently demonstrated that the activity of factor XIII is indeed changed close to the electrode surface.[39] We thus consider the electrochemical degradation of Fg and the consequent loss of Fg clottability to be an important mechanism explaining the reduced coagulation at the cathode, but not the only one.

Finally, to investigate if the formation of reactive oxygen species was involved in the desorption process, we performed the desorption experiment in oxygen-depleted atmosphere. We did not observe changes in the frequency signal compared to previous experiments in air (Supporting Information Figure S8), suggesting negligible contribution of such reactive groups in the degradation process.

CONCLUSIONS

Electrodes might contact blood in various situations. Examples include, but are not limited to, their use *in vivo* as stimulators and their *in vivo* and *in vitro* uses as sensors for substances present in blood. Understanding the interfacial thrombosis mechanism and the electrochemical reactions involving plasma proteins at the electrode surface is of fundamental importance to improve the design of electrodes in contact with blood and the way these are operated. Our understanding of the role of cathodic currents in reducing interfacial thrombosis considerably increased. We found that Fg electrochemically desorbs from the cathode and loses an important polymerization site located at one of its termini, affecting its ability to clot. This is most likely due to the local alkali peptide hydrolysis induced by the electrode, but more experiments have to be designed to provide stronger evidence on the direct or indirect electrochemical reaction(s) responsible for this observation. The conversion from Fg to fibrin and the fibrin deposition on the surface are fundamental steps leading to thrombosis. However, future studies should focus on the electrochemical reactions involving other fundamental blood coagulation factors. In fact, a large part of this study was carried out using solutions of purified Fg; therefore, the validity of our conclusion in blood plasma, a solution containing hundreds of different proteins competing for the surface, is somewhat limited. For these reasons, the results presented here should be used with caution when comparisons with different systems (both *in vivo* and *in vitro*) will be made.

ACKNOWLEDGMENTS

The authors thank Stephen Wheeler (IBT-ETH Zurich workshop) for manufacturing the custom-made QCM modules. SEM was performed at the Center of Microscopy and Image Analysis (ZMB, ETH and University of Zurich). B.R.S. thanks Dr. Andres Kaech and Klaus Marquardt for teaching and support. The authors thank Prof. Quan Jason Cheng (University of California, Riverside) for discussions. MS was performed at the Functional Genomics Center Zurich (FGCZ, University and ETH Zurich), and the staff is acknowledged for teaching and support. This work was financially supported by ETH and University Zurich.

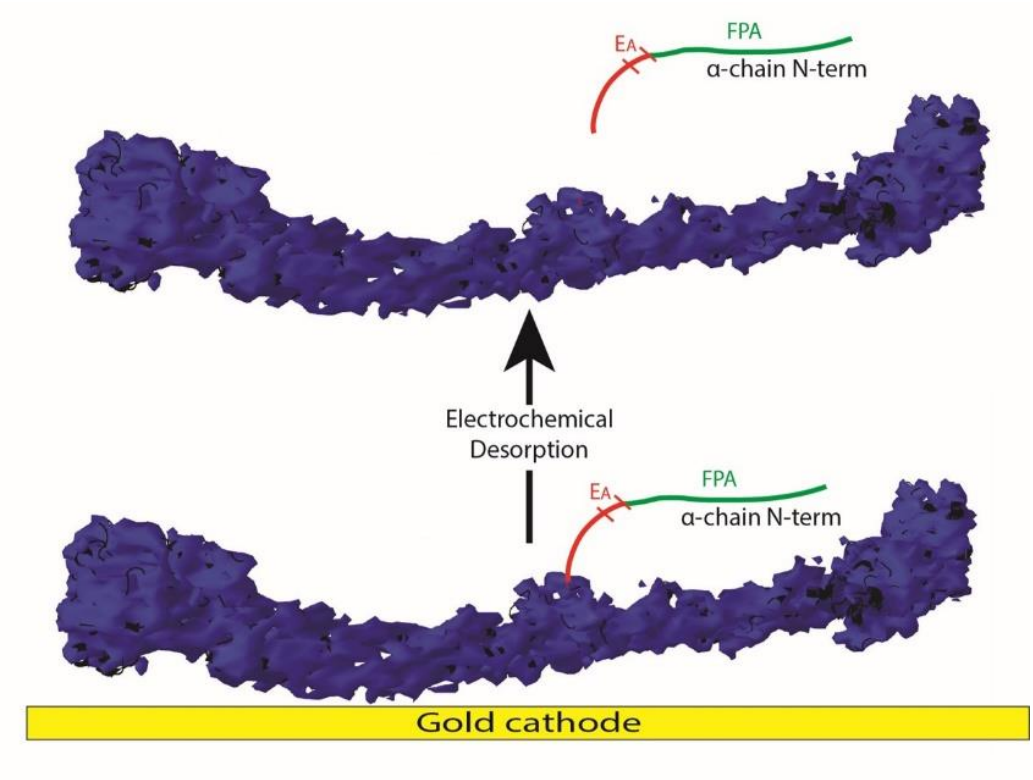

Figure 6. Schematic representation of the Fg molecule with the flexible N-terminus of the α-chain starting with the FPA and containing the polymerization site EA. Only one of the two α-chain N-termini is represented for better clarity. Upon electrochemical desorption from the cathode, the flexible N-terminus is cleaved. The 3D representation was adapted from Kollman et al.,[40] and the mobile α-chain N-terminus was drawn manually because its 3D coordinates have not been determined.

REFERENCES

[1] Bailly A-L, Laurent A, Lu H, Elalami I, Jacob P, Mundler O, et al. Fibrinogen binding and platelet retention: Relationship with the thrombogenicity of catheters. Journal of Biomedical Materials Research. 1996;30:101-8.

[2] Ratner BD. The blood compatibility catastrophe. Journal of Biomedical Materials Research. 1993;27:283-7.

[3] Vogler EA, Siedlecki CA. Contact activation of blood-plasma coagulation. Biomaterials. 2009;30:1857-69.

[4] Ratner BD. The catastrophe revisited: Blood compatibility in the 21st Century. Biomaterials. 2007;28:5144-7.

[5] Vogler EA. Protein adsorption in three dimensions. Biomaterials. 2012;33:1201-37.

[6] Horbett TA. Chapter 13 Principles underlying the role of adsorbed plasma proteins in blood interactions with foreign materials. Cardiovascular Pathology. 1993;2:137-48.

[7] Hansson KM, Tosatti S, Isaksson J, Wetterö J, Textor M, Lindahl TL, et al. Whole blood coagulation on protein adsorption-resistant PEG and peptide functionalised PEG-coated titanium surfaces. Biomaterials. 2005;26:861-72.

[8] Zhang Z, Zhang M, Chen S, Horbett TA, Ratner BD, Jiang S. Blood compatibility of surfaces with superlow protein adsorption. Biomaterials. 2008;29:4285-91.

[9] Smith RS, Zhang Z, Bouchard M, Li J, Lapp HS, Brotske GR, et al. Vascular Catheters with a Nonleaching Poly-Sulfobetaine Surface Modification Reduce Thrombus Formation and Microbial Attachment. Science Translational Medicine. 2012;4:153ra32.

[10] Gott VL, Whiffen JD, Dutton RC. Heparin bonding on colloidal graphite surfaces. Science 1963;142:1297-8.

[11] Hoshi RA, Van Lith R, Jen MC, Allen JB, Lapidos KA, Ameer G. The blood and vascular cell compatibility of heparin-modified ePTFE vascular grafts. Biomaterials. 2013;34:30-41.

[12] Shankar H, Senatore F, Zuniga P, Venkataramani E. Enhanced in vitro fibrinolytic activity of immobilized plasmin on collagen beads. Journal of Biomedical Materials Research. 1987;21:897-912.

[13] Chen H, Wang L, Zhang Y, Li D, McClung WG, Brook MA, et al. Fibrinolytic Poly(dimethyl siloxane) Surfaces. Macromolecular Bioscience. 2008;8:863-70.

[14] Li D, Chen H, Brash JL. Mimicking the fibrinolytic system on material surfaces. Colloids and Surfaces B: Biointerfaces. 2011;86:1-6.

[15] Alfonsi-Hourdin S, Longchamp S, Gallet O, Nigretto J-M. Electrochemical processing of fibrinogen modified-graphite surfaces: Effect on plasmin generation from adsorbed plasminogen. Biomaterials. 2006;27:52-60.

[16] McGuigan AP, Sefton MV. The influence of biomaterials on endothelial cell thrombogenicity. Biomaterials. 2007;28:2547-71.

[17] Pernagallo S, Tura O, Wu M, Samuel K, Diaz-Mochon JJ, Hansen A, et al. Novel Biopolymers to Enhance Endothelialisation of Intra-vascular Devices. Advanced Healthcare Materials. 2012;1:646-56.

[18] Yu K, Lai BFL, Kizhakkedathu JN. Carbohydrate Structure Dependent Hemocompatibility of Biomimetic Functional Polymer Brushes on Surfaces. Advanced Healthcare Materials. 2012;1:199-213.

[19] Yang Q, Tian J, Hu M-X, Xu Z-K. Construction of a Comb-like Glycosylated Membrane Surface by a Combination of UV-Induced Graft Polymerization and Surface-Initiated ATRP. Langmuir : the ACS journal of surfaces and colloids. 2007;23:6684-90.

[20] Mani G, Feldman MD, Patel D, Agrawal CM. Coronary stents: A materials perspective. Biomaterials. 2007;28:1689-710.

[21] Ramasamy N, Ranganathan M, Duic L, Srinivasan S, Sawyer PN. Electrochemical Behavior of Blood Coagulation Factors. Journal of The Electrochemical Society. 1973;120:354.

[22] Lucas TR, Stanczewski B, Ramasamy N, Srinivasan S, Kammlott GW, Sawyer PN. Nonthrombogenic ac Polarized Copper Prosthesis. Artificial Cells, Blood Substitutes and Biotechnology. 1975;3:215-32.

[23] Chopra PS, Srinivasan S, Lucas T, Sawyer PN. Relation between Thrombosis on Metal Electrodes and the Position of Metal in the Electromotive Series. Nature. 1967;215:1494-.

[24] Mosesson MW. Fibrinogen and fibrin structure and functions. Journal of Thrombosis and Haemostasis. 2005;3:1894-904.

[25] Lambrecht LK, Young BR, Stafford RE, Park K, Albrecht RM, Mosher DF, et al. The influence of preadsorbed canine von willebrand factor, fibronectin and fibrinogen on ex vivo artificial surface-induced thrombosis. Thrombosis Research. 1986;41:99-117.

[26] Grunkemeier JM, Tsai WB, Horbett TA. Co-adsorbed fibrinogen and von Willebrand factor augment platelet procoagulant activity and spreading. Journal of Biomaterials Science Polymer Edition. 2001;12:1-20.

[27] Stoner G, Walker L. Enzymatic and electrochemical polymerization of fibrinogen. Journal of Biomedical Materials Research. 1969;3:645-54.

[28] Mallon CT, De Chaumont C, Moran N, Keyes TE, Forster RJ. Electrochemical desorption of fibrinogen from gold. Langmuir : the ACS journal of surfaces and colloids. 2010;26:293-8.

[29] Vikinge TP, Hansson KM, Sandström P, Liedberg B, Lindahl TL, Lundström I, et al. Comparison of surface plasmon resonance and quartz crystal microbalance in the study of whole blood and plasma coagulation. Biosensors and Bioelectronics. 2000;15:605-13.

[30] Andersson M, Andersson J, Sellborn A, Berglin M, Nilsson B, Elwing H. Quartz crystal microbalance-with dissipation monitoring (QCM-D) for real time measurements of blood coagulation density and immune complement activation on artificial surfaces. Biosensors & bioelectronics. 2005;21:79-86.

[31] Funck T, Eggers F. Clotting of blood at a gold surface probed by MHz shear quartz resonator. Naturwissenschaften. 1982;69:499-501.

[32] Permentier HP, Bruins AP. Electrochemical oxidation and cleavage of proteins with on-line mass spectrometric detection: development of an instrumental alternative to enzymatic protein digestion. Journal of the American Society for Mass Spectrometry. 2004;15:1707-16.

[33] Rzany A, Schaldach M. Physical Properties of Antithrombogenic Materials – An Electronic Model of Contact Activation. Progress in Biomedical Research. 1999;4:59-70.

[34] Langer SH, Landi HP. The Nature of Electrogenerative Hydrogenation. Journal of the American Chemical Society. 1964;86:4694-8.

[35] Keil B, Zikán J, Rexová L, Sorm F. Hydrogenation of aromatic amino acids in peptides. Collection of Czechoslovak Chemical Communications. 1962;27:1678-86.

[36] Gabi M, Sannomiya T, Larmagnac A, Puttaswamy M, Voros J. Influence of applied currents on the viability of cells close to microelectrodes. Integrative Biology. 2009;1:108-15.

[37] Machovich R. The Thrombin: CRC Press; 1984.

[38] Ehrbar M, Rizzi SC, Hlushchuk R, Djonov V, Zisch AH, Hubbell JA, et al. Enzymatic formation of modular cell-instructive fibrin analogs for tissue engineering. Biomaterials. 2007;28:3856-66.

[39] Milleret V, Simona BR, Lienemann PS, Vörös J, Ehrbar M. Electrochemical Control of the Enzymatic Polymerization of PEG Hydrogels: Formation of Spatially Controlled Biological Microenvironments. Advanced Healthcare Materials. 2014;3:508-14.

[40] Kollman JM, Pandi L, Sawaya MR, Riley M, Doolittle RF. Crystal Structure of Human Fibrinogen. Biochemistry. 2009;48:3877-86.

SUPPORTING INFORMATION

Coagulation at the Blood-Electrode Interface: The Role of Electrochemical Desorption and Degradation of Fibrinogen

Benjamin R. Simona[†], René A. Brunisholz[‡], Robert Morhard[†], Peter Hunziker[‡] and János Vörös[†]*

[†]*Laboratory of Biosensors and Bioelectronics, Institute for Biomedical Engineering, University and ETH Zurich, Gloriastrasse 35, CH-8092 Zurich, Switzerland.*

[‡]*Functional Genomics Center Zurich, University and ETH Zurich, Winterthurerstrasse 190, CH-8057 Zurich, Switzerland.*

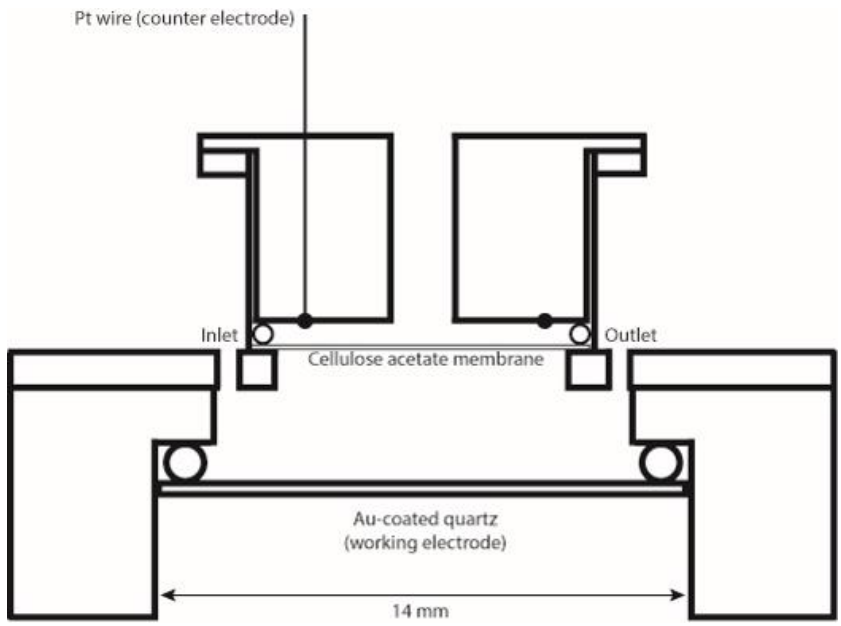

Suppl. Figure S1. Cross section of the home-made electrochemical QCM cell. Technical drawings available on request.

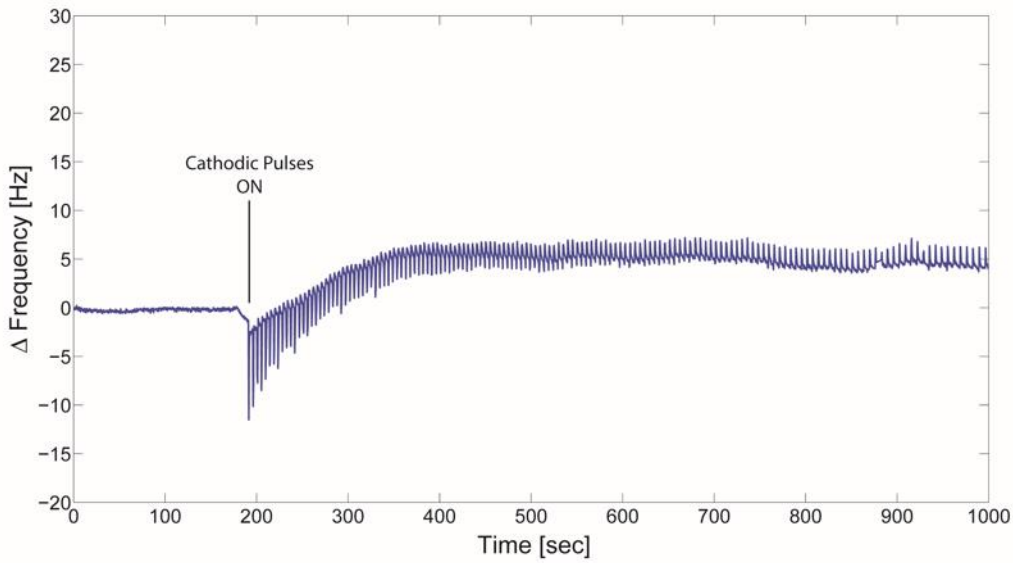

Suppl. Figure S2. Frequency signal measured in 100 mM NaCl upon the application of a cathodic square wave pulsed current (I = -1 mA/cm^2, τ_{ON} = 1 sec, τ_{OFF} = 5 sec).

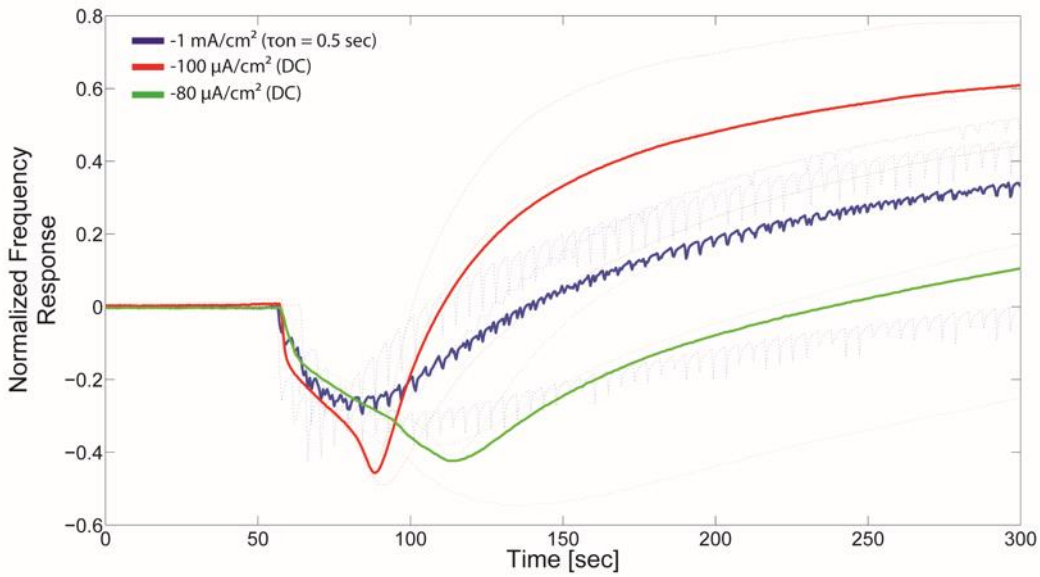

Suppl. Figure S3. Dependency of Fg electrochemical desorption on current intensity (see Figure 2).

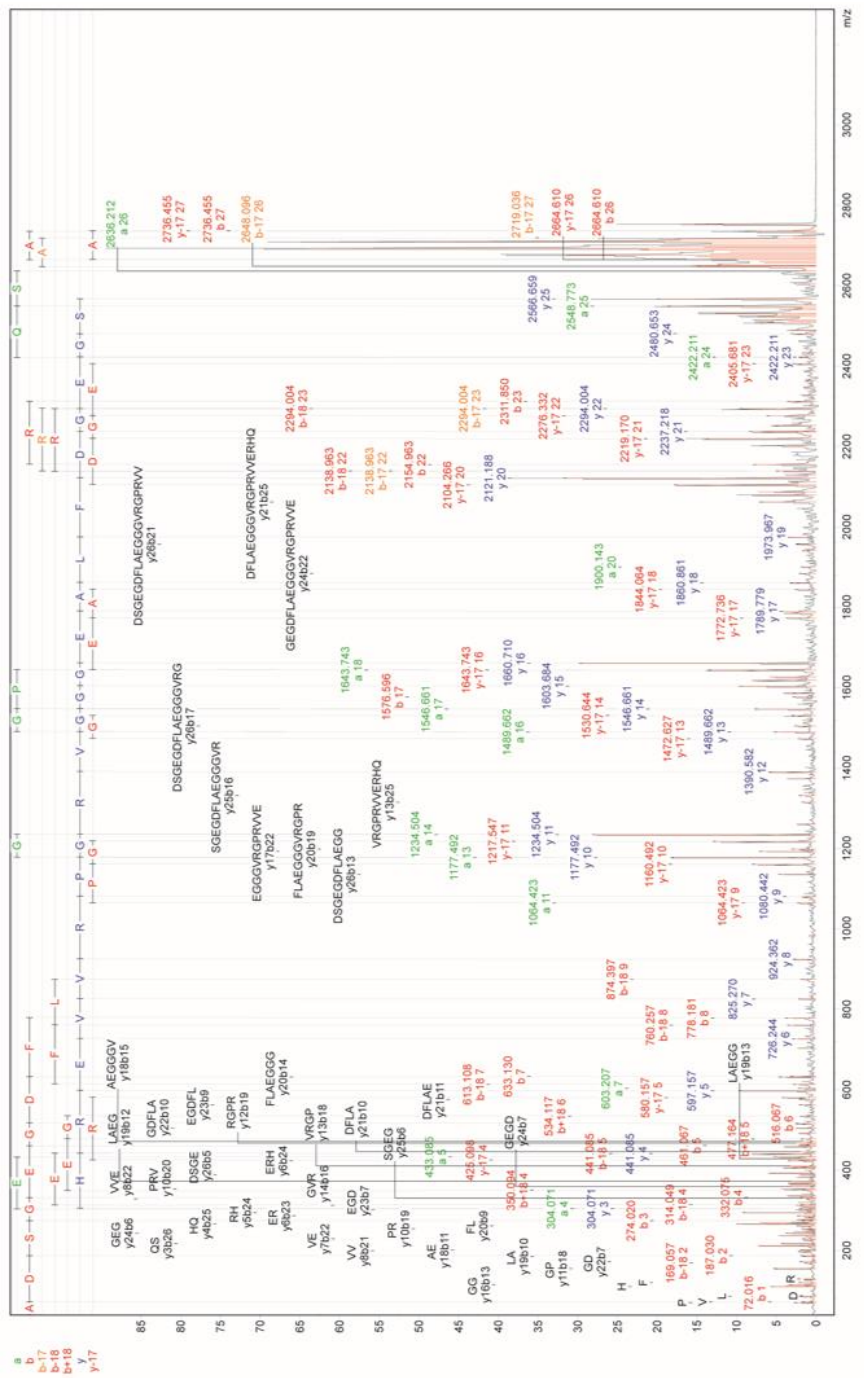

Suppl. Figure S4. MALDI-TOFTOF MS spectrum of the 2752.3 Da precursor.

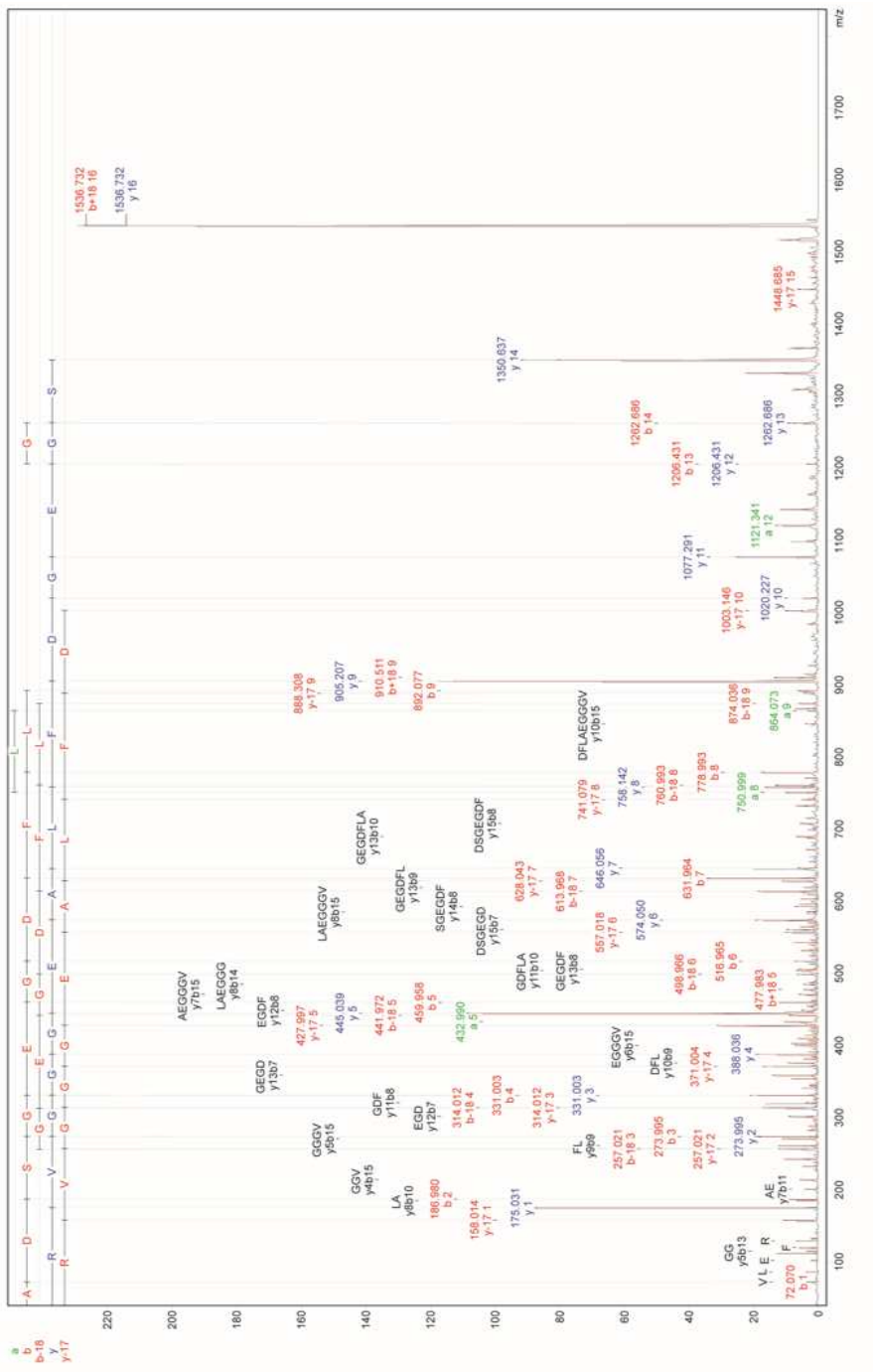

Suppl. Figure S5. MALDI-TOFTOF MS spectrum of the 1536.7 Da precursor.

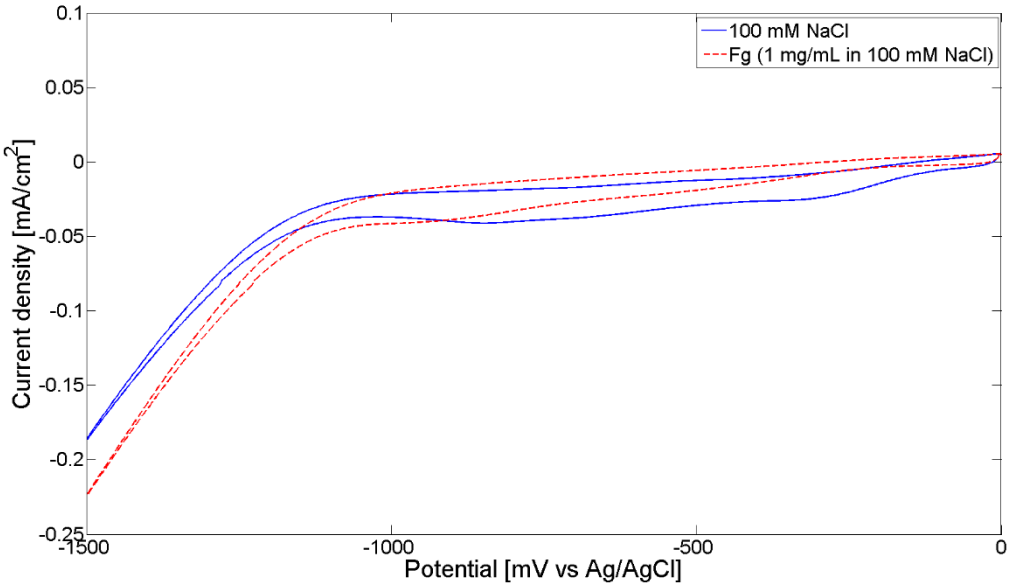

Suppl. Figure S6. Cyclic voltammogram of the gold-coated QCM crystal in 100 mM NaCl before and after addition of Fg (1 mg/mL). The potential was swept for 15 minutes at the corresponding condition and then recorded. The platinum counter electrode and the Ag/AgCl pseudo-reference were separated from the gold working electrode by the acetate cellulose membrane impermeable to Fg.

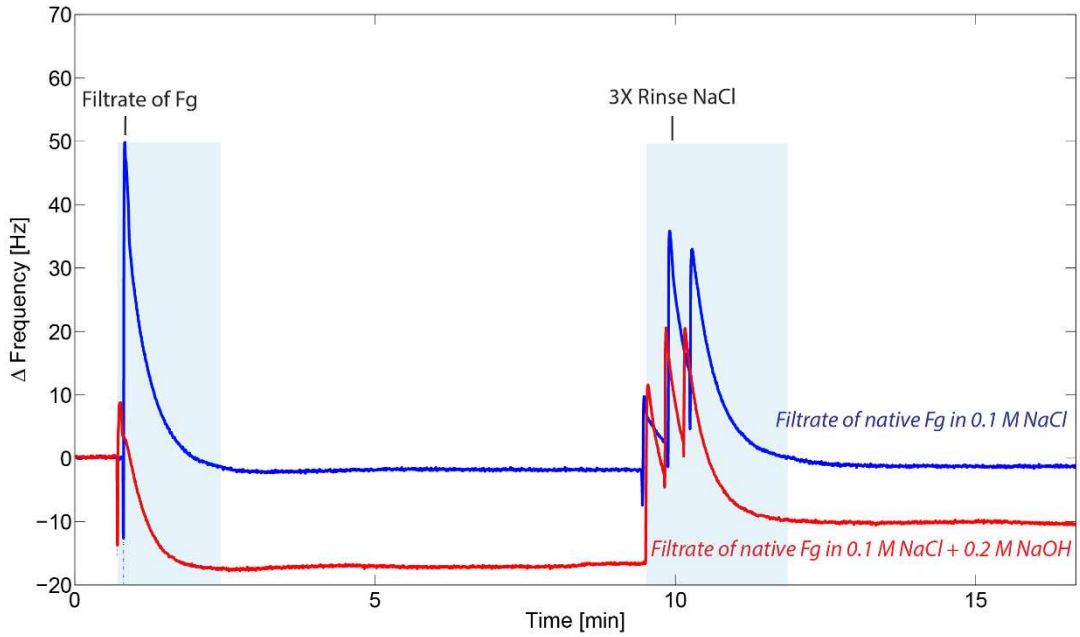

Suppl. Figure S7. Adsorption of the filtrate of native Fg incubated overnight at room temperature with 0.2 M NaOH and without NaOH. After incubation of the Fg in 0.2 M NaOH, the solution was neutralized by adding HCl. Centrifugal filtration was subsequently performed through 30 kDa MWCO membranes as done in Fig. 3. The baseline was acquired in 0.1 M (0 M NaOH) and 50 µL of the Fg filtrates were injected. After stabilization of the frequency signal, the chambers were rinsed 3X with 0.1 M NaCl (0 M NaOH). The shaded blue areas show the frequency change due to temperature stabilization.

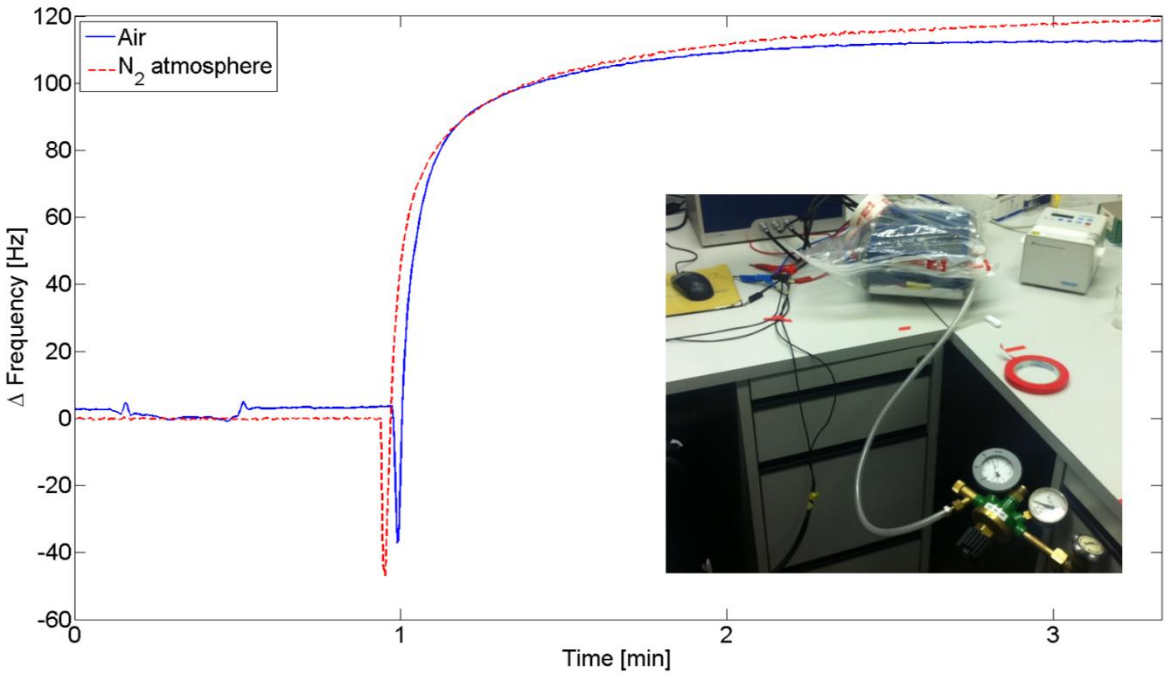

Suppl. Figure S8. Electrochemical desorption experiment in Oxygen-depleted atmosphere. 1 mg/mL Fg solution was prepared in 100 mM NaCl previously de-aired in vacuum for 2 hours and bubbled with a Nitrogen gun for 10 minutes. The electrochemical desorption experiment of Fig. 2 (-1mA/cm^2, DC) was repeated. The Q-Sense E4 chamber was placed in a plastic bag and was perfused with a constant Nitrogen flow starting 15 minutes before the experiment and during the desorption.

Tables

Current Density [µA/cm^2]	**Potential [mV vs Ag/AgCl]**
-10	-220
-1000	-2161

Suppl. Table S1. Potential measured after 2 min of application of the minimal and maximal current density (DC) used in this study. The potential was stable and measured in a 3-electrode setup against a pseudo-reference Ag/AgCl. The platinum counter electrode and the Ag/AgCl pseudo-reference were separated by the gold working electrode from the acetate cellulose membrane.

N-Term	Ion	b ion	y ion	Ion	C-Term
20	A	**72.044**	90.055	A	46
21	D	**187.071**	177.087	S	45
22	S	**274.103**	**305.146**	Q	44
23	G	**331.125**	**442.204**	H	43
24	E	**460.167**	**598.306**	R	42
25	G	**517.189**	**727.348**	E	41
26	D	**632.216**	**826.417**	V	40
27	F	**779.284**	**925.485**	V	39
28	L	892.368	**1081.856**	R	38
29	A	963.405	**1178.639**	P	37
30	E	1092.448	**1235.660**	G	36
31	G	1149.469	**1391.761**	R	35
32	G	1206.491	**1490.830**	V	34
33	G	1263.512	**1547.851**	G	33
34	V	1362.581	**1604.873**	G	32
35	R	1518.682	**1661.894**	G	31
36	G	**1575.703**	**1790.937**	E	30
37	P	1672.756	**1861.974**	A	29
38	R	1828.857	**1975.058**	L	28
39	V	1927.926	**2122.126**	F	27
40	V	2026.994	**2237.153**	D	26
41	E	**2156.037**	**2294.175**	G	25
42	R	**2312.138**	**2423.217**	E	24
43	H	2449.197	**2480.239**	G	23
44	Q	2577.255	**2567.271**	S	22
45	S	**2664.287**	2682.298	D	21
46	A	**2735.324**	2753.335	A	20

Suppl. Table S2. MALDI-TOFTOF MS of the electrochemically generated Fg degradation product. Theoretical masses of the fragmented 2752.3 Da peptide are shown. The experimental values matching the theoretical fragmentation values are marked in bold. The 2752.3 Da precursor was identified as the mobile N-terminus of the Fg α-chain starting with the FPA and terminating with the Ala-46. Importantly, this sequence includes the Fg α-chain E_A constituted of the Gly-Pro-Arg-Val (36-39) motif. The spectra of the 2752.3 Da and of the 1536.7 Da precursors are shown in Suppl. Figures S4 and S5. The amino acid numeration starts at position 20 (N-term) because it includes the signalling peptide (1-20) not present in the mature protein.

N-Term	Ion	b ion	y ion	Ion	C-Term
20	A	**72.044**	**175.119**	R	35
21	D	**187.071**	**274.187**	V	34
22	S	**274.103**	**331.209**	G	33
23	G	**331.125**	**388.230**	G	32
24	E	**460.167**	**445.252**	G	31
25	G	**517.189**	**574.294**	E	30
26	D	**632.216**	**645.331**	A	29
27	F	**779.284**	**758.416**	L	28
28	L	**892.368**	**905.484**	F	27
29	A	963.405	**1020.511**	D	26
30	E	1092.448	**1077.532**	G	25
31	G	1149.469	**1206.575**	E	24
32	G	**1206.491**	**1263.596**	G	23
33	G	**1263.512**	**1350.628**	S	22
34	V	1362.581	1465.655	D	21
35	R	1518.682	**1536.692**	A	20

Suppl. Table S3. MALDI-TOFTOF MS of the Fibrinopeptide A (FPA). Theoretical masses of the fragmented 1536.7 Da peptide are shown. The experimental values matching the theoretical fragmentation values are marked in bold. The amino acid numeration starts at position 20 (N-term) because it includes the signalling peptide (1-20) not present in the mature protein.